SIMULATION OF IONS ACCELERATION AND EXTRACTION IN CYCLOTRON C400

Y. Jongen, W. Kleeven, IBA, Louvain-la-Neuve, Belgium, G. Karamysheva, N. Morozov, S. Kostromin, E. Samsonov, JINR, Dubna, Russia

Abstract

The Belgian company IBA, together with scientists of JINR (Dubna) is designing a superconducting isochronous cyclotron [1] for carbon and proton beam therapy. The new cyclotron C400 is to deliver carbon ions $^{12}C^{6+}$ with energy 400 MeV/amu and protons with energy close to 260 MeV.

INTRODUCTION

The cyclotron has a compact type superconducting magnet [2] with a pole of radius 187 cm. The axial focusing is provided by four sectors, with a spiral angle increasing to the maximum value close to 70° at the maximum energy. With this design, the axial betatron frequency is maintained during most of the acceleration.

The beam acceleration is provided by two spiral dees located in opposite valleys. The dee voltage increases from 100 kV at the center to 200 kV at the extraction. The paper presents the analysis of the beam acceleration in the proposed new cyclotron. During the acceleration, several resonance lines occur, but the simulation demonstrates that these resonances are crossed without essential damaging the beam properties.

Carbon ions are extracted by using an electrostatic deflector followed by two magnetic correctors. Protons are extracted at lower energy by stripping of $^{2}H^{1+}$ ions.

Simulation has been mainly performed with our codes CYCMOT and EXTMOT which make the ions tracking calculations in a six dimensional phase volume for the acceleration and extraction regions, respectively.

MAGNETIC FIELD ISOCHRONIZATION

A two-step procedure was used to isochronize the average magnetic field of cyclotron. At the first step we applied approximation [3], taking into account the azimuthal field variation obtained from the TOSCA model [2]. At the second step the ion acceleration from the center to the final radius was simulated. The RF phase of the ion was calculated during this simulation but was not taken into account for energy gain estimation in the accelerating gaps. This condition made it possible to accelerate ion to the final radius and to obtain the next approximation to the required average field:

$$\overline{B}_{new}(r) = \overline{B}_{old}(r)\left(1+\frac{\Delta\varphi_{RF}(r)}{2\pi h}\right),$$ where

$\overline{B}_{old}, \overline{B}_{new}$ are the old and new distributions of the average field along the radius, $\Delta\varphi_{RF}$ is the phase advance in one turn, $h=4$ is the harmonic number.

With four iterations it was possible to obtain the average field, which ensures the constancy of the ion phase with accuracy ±10°RF. Figure 1 shows the radial dependence of the ion orbital frequency and ion phase in the resulting field. In contrast to the foregoing computations these results were obtained when the ion RF phase was taken into account in the energy gain calculation. About 1300 turns were needed to get the final radius.

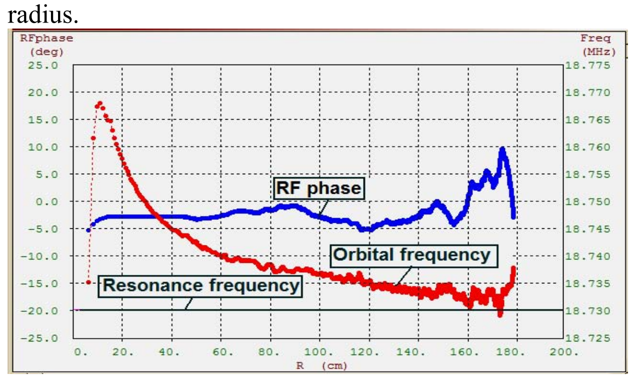

Figure 1: Radial dependence of the ion orbital frequency and RF phase in the resulting magnetic field.

These results were obtained using ion acceleration along the shims and dees spirality. One sees in Figure 1 that the orbital frequency is larger than the resonance one in the whole acceleration region. In spite of this fact the ion RF phase stays within the appropriate limits. The radial component of the accelerating field provides a condition when the increased orbital frequency almost exactly compensates [4] the RF phase advance arisen due to dees spirality.

BETATRON RESONANCES

During acceleration the ions cross the lines of 17 resonances (Figure 2). We derived the equilibrium orbits and the betatron frequencies ν_r and ν_z using the field map obtained from the TOSCA model [2].

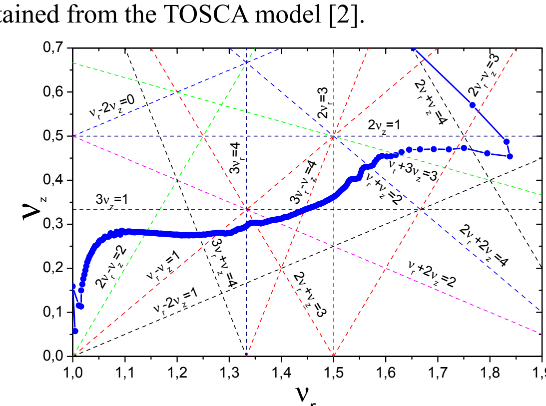

Figure 2: Working point diagram of the cyclotron.

All resonances can be subdivided into two groups. The first group consists of 6 internal resonances $n\nu_r \pm k\nu_z = 4$ having the main 4th harmonic of the magnetic field as a driving term. The second group includes 11 external resonances $n\nu_r \pm k\nu_z = m$, m=0, 1, 2, 3 that could be excited by the magnetic field perturbations. So far 12 resonances have been studied. The remaining 5 resonances located at the center and edge regions of cyclotron will be studied in the near future when the magnetic field here will have been optimized.

The computations have shown that the most dangerous resonances are $3\nu_r = 4$ and $\nu_r - \nu_z = 1$. Action of the remaining resonances either is unnoticeable for the amplitudes of free oscillations up to 8-10 mm or the tolerances for magnetic field perturbations in the vicinity of resonances are not less than few tenths of gauss, which is easily provided in practice.

Resonance $3\nu_r = 4$

This resonance, occurring on the radius 154.6 cm, is excited by the 4th harmonic of azimuthal variation in the magnetic field. The limiting amplitude of the radial oscillations of ions, which corresponds to the stability of radial motion around the resonance in the static regime, was determined for the first time. One sees in Figure 3 that the limiting amplitude of the radial oscillations of ions in this regime is equal to 0.3 cm.

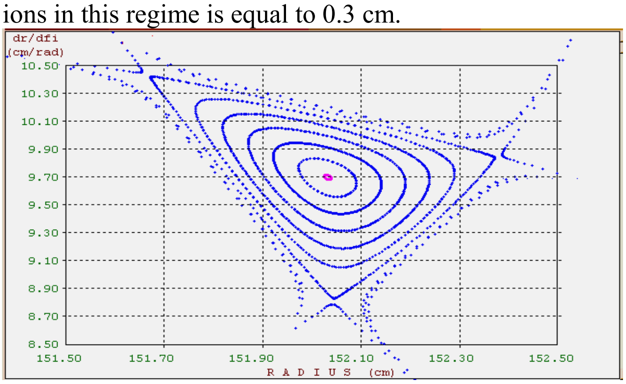

Figure 3: Static motions of 9 ions on radial phase plane. Range of starting radial amplitudes is 0.0 – 0.4 cm with step 0.05 cm.

Then acceleration of 500 ions randomly distributed inside three dimensional phase volume (r, p_r, RFphase) was simulated.

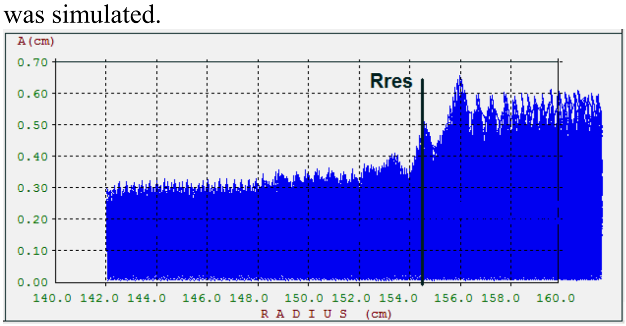

Figure 4: Amplitudes of radial oscillations versus the average radius of the orbits in the resonance region. U_{dee}=90 kV.

Initial position of the ions in the radial phase plane corresponded to 4 different distributions of the radial amplitudes: up to 0.1, 0.2, 0.3 and 0.4 cm. Two different values of the dee voltage in the vicinity of resonance, 90 and 180 kV were used in the simulation. Figure 4 illustrates the results of these computations for the bunch with the initial amplitude 0.3 cm and for the dee voltage 90 kV. It is seen that the radial motion under the imposed conditions remains stable but the resulting radial amplitude becomes two times greater than it was before the resonance. Impact of the resonance on the radial motion can be partly corrected by means of the average magnetic field perturbation of special form (Figure 5) which ensures an increase of the derivative $d\nu_r/dr$ at the resonance crossing.

This perturbation (created by small changes in the sectors geometry) shifts the resonance radius from 154.6 cm to 155.6 cm and permits to enlarge $d\nu_r/dr$ by a factor of two.

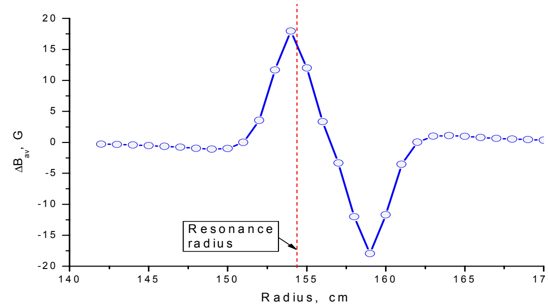

Figure 5: Radial distribution of the average field perturbation with zero RF phase advance.

Based on the results of computations for the unperturbed and perturbed average magnetic field as well as for the increased dee voltage, the resulting radial amplitude after resonance crossing was plotted (Figure 6) as a function of the initial one (before the resonance).

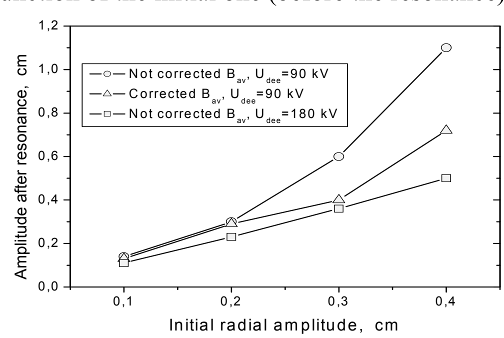

Figure 6: Resulting radial amplitude after the resonance versus initial radial amplitude.

One observes that the field perturbation (Figure 5) noticeably decreases the amplitudes of radial oscillations. However, the increase in the radial amplitudes can be most effectively limited by the dees voltage enlargement.

Resonance $\nu_r - \nu_z = 1$

A driving term of this resonance occurred on r=146 cm is the 1st harmonic B_{1r} of the radial magnetic field perturbation, which could be caused, for example, by main coil tilt. A number of computations were done varying the amplitude of initial radial oscillations and the maximal value of $B_{1r}(r)$ and using different types of B_{1r} radial distribution. A typical view of the beam axial size along the radius which corresponds to two B_{1r} radial distributions with the maximal B_{1r}=10 G is shown in Figure 7.

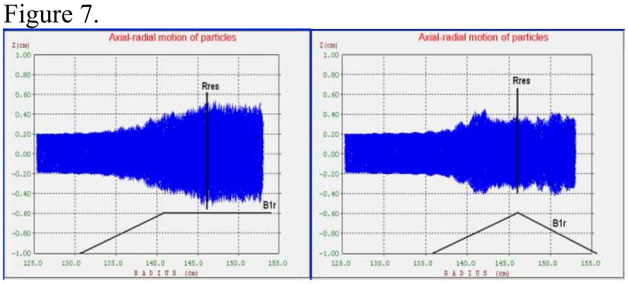

Figure 7: Projection of the beam on the radial-axial plane marked four times in each of 400 turns. The radial amplitude is 3 mm. Two different forms of $B_{1r}(r)$ were used.

The larger the beam radial amplitudes, the larger the B_{1r} impact on the axial amplitudes. For the proposed radial oscillation 3 mm the increase in the beam axial size by not more than 50% after the resonance crossing is provided if the maximum of $B_{1r}(r)$ is not larger than 5-7 G, depending on the form of the B_{1r} radial distribution near the resonance.

BEAM EXTRACTION

Carbon ions will be extracted by an electrostatic deflector followed by two magnetic correctors. The appropriate beam radial gain per turn (~3 mm) at entrance of the deflector is provided by both the energy gain and by the betatron motion. For the beam with betatron amplitudes up to 3 mm, the RMS emittances at the deflector entrance (Figure 8) are ε_r = 0.25 π mm•mrad, ε_z =0.86 π mm•mrad, energy is W=400.7±0.4 MeV/amu.

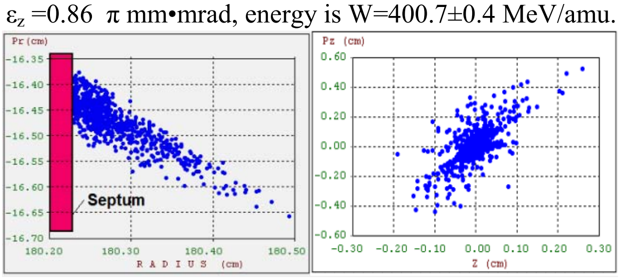

Figure 8: Beam portraits (1000 ions) on the radial and axial phase planes at the deflector entrance.

To avoid the beam axial losses arisen due to the resonances $2\nu_r+\nu_z=4$ and $2\nu_z=1$, (see Figure 2), the extraction is done before these resonances crossing. The uniform electric field 140 kV/cm inside the deflector is needed to provide the beam extraction. Two passive magnetic correctors with the field gradient 4 T/m are used for the beam focusing in the horizontal plane. The plan view of cyclotron pole with the dees and extraction system is presented in Figure 9. About 25% of the beam is lost in the entrance part of the septum having the thickness 0.3 mm. Beam envelopes (Figure 10) are limited so that no beam losses are observed inside the extraction system.

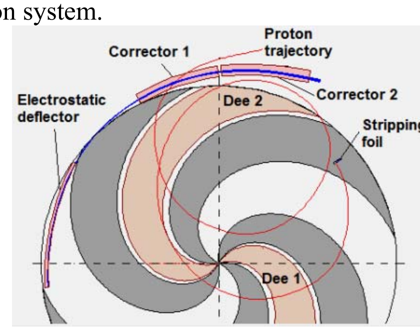

Figure 9: Layout of the cyclotron with extraction of two beams. Direction of acceleration along spirality was chosen taking into account the beam focusing in the horizontal plane inside the deflector provided by the main magnetic field (see Figure 10, left graph).

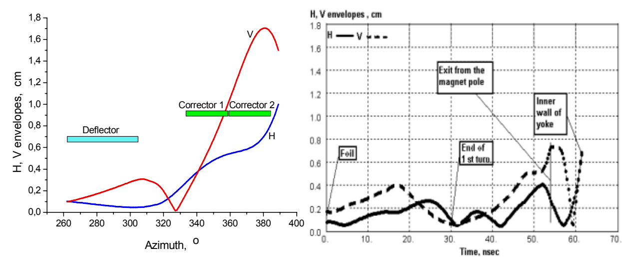

Figure 10: Beam envelopes of the carbon beam (left) versus azimuth and of the proton beam (right) versus time.

Extraction of protons with energy ~260 MeV is ensured by stripping of $^2H^{1+}$ ions. Two-turn scheme of the protons motion after the stripping foil (Figure 9) is proposed to deliver the beam outside the cyclotron magnet. Beam envelopes during time of these two turns are shown in Figure 10. No focusing elements are needed to get the beam at the inner wall of the magnet yoke. The first corrector must have a hole in its construction for the passage of proton beam. Convergence of $^{12}C^{6+}$ and proton beams into one transport line will be achieved beyond the magnet of cyclotron.

REFERENCES

[1] Y.Jongen et al., “Design Studies of the Compact Superconducting Cyclotron for Hadron Therapy”, this conference.

[2] Y.Jongen et al., “Computer Modelling of Magnetic System for C400 Superconducting Cyclotron”, this conference.

[3] M.M.Gordon, “Calculation of Isochronous Fields for Sector-focused Cyclotrons”, Particle accelerators, 13, (1983), p. 67.

[4] M.M.Gordon, “Effects of Spiral Electric Gaps in Superconducting Cyclotrons”, NIM, 169(1980), p. 327-336.